

Semiconductor Electrodes

LV. Differential Photocurrent Determination of Absorption Coefficient and Diffusion Length in p-GaP Photoelectrochemical Cells

Bob L. Wheeler, G. Nagasubramanian, and Allen J. Bard

Department of Chemistry, The University of Texas at Austin, Austin, Texas 78712

ABSTRACT

The differential photocurrent (DPC) method, which involves simultaneous modulation of the incident radiation (at f_1) and the applied potential (at f_2) with detection of the intermodulation photocurrent (at $|f_2 - f_1|$), was employed in the determination of α and L for p-GaP in contact with aqueous solutions of Eu^{3+} . Typical values of α determined by this technique were (450 nm) $6.9 \times 10^4 \text{ cm}^{-1}$ and (400 nm) $8.1 \times 10^4 \text{ cm}^{-1}$. The value of L obtained was $0.10 \pm 0.01 \mu\text{m}$, which is smaller than that found for high purity p-GaP in solid-state devices and is attributed to traps or recombination centers in the p-GaP electrode material.

Radiant-to-electrical energy conversion at a semiconductor electrode in contact with an electrolyte in a liquid junction photoelectrochemical (PEC) cell is often controlled by the optical absorption coefficient, α , and the minority carrier diffusion length, L , of the semiconductor. In principle, by measuring the photocurrent under monochromatic illumination as a function of potential, one can obtain the necessary information for the computation of α and L . The Gärtner model and its variations (1-5) are the simplest models for the photocurrent density, j , at the semiconductor/liquid interface. This model assumes that minority carriers generated within the electric field of the space-charge layer (scl) are swept to the interface where they react; recombination within the scl is neglected. Carriers generated outside the scl must diffuse to it. Only those carriers within a distance L of the edge of the scl [where $L = (D\tau)^{1/2}$; D is the diffusion coefficient and τ is the lifetime of the minority carriers] are swept to the interface. More rigorous and complex models for the photocurrent have been proposed (4, 5); these include the effects of surface recombination, bulk and scl recombinations, slow charge-transfer kinetics at the interface, etc. These models are much more difficult to apply to actual experimental studies, however, because they involve many adjustable parameters and numerical solutions or digital simulations rather than analytical solutions. Hence, the Gärtner-like model is frequently used, and we apply this model here in a first attempt at determining α and L by the differential photocurrent (DPC) method—a method first proposed for solid-state devices by Sukegawa *et al.* (6).

The Gärtner equation can be written (1-3)

$$j = KqI\{1 - [e^{-\alpha w}/(1 + \alpha L)]\} \quad [1]$$

where w is the thickness of the scl and is a function of the potential, V , with respect to the flatband potential V_{FB} , and is given by

$$w = [(2\epsilon\epsilon_0/qN)(|V - V_{\text{FB}}|)]^{1/2} \quad [2]$$

ϵ is the dielectric constant of the semiconductor and ϵ_0 is the permittivity of free space, N is the donor or acceptor density, and V is the applied potential with respect to the flatband, V_{FB} . When an ac voltage of amplitude V_0 is superimposed on the dc potential, the variation in space-charge layer thickness, Δw , is given by

$$\Delta w = \epsilon\epsilon_0 V_0 / qNw \quad [3]$$

These equations were used by Sukegawa *et al.* (6). In Eq. [1], K includes terms that are independent of V and the intensity, I , such as the reflectivity of the electrode, etc. The photocurrent density can thus be represented as a function of $|V - V_{\text{FB}}|$ or w (Fig. 1). As

* Electrochemical Society Active Member.

$w \rightarrow \infty$; $j \rightarrow j_{\text{sat}} = KqI$. At $V = V_{\text{FB}}$ or $w = 0$, j is given by

$$[j]_{w=0} = KqI[\alpha L/(1 + \alpha L)] \quad [4]$$

The slope of the j vs. w curve at any point is given by

$$(dj/dw) = KqI\alpha e^{-\alpha w}/(1 + \alpha L) \quad [5]$$

In particular, at $w = 0$

$$(dj/dw)_{w=0} = KqI\alpha/(1 + \alpha L) \quad [6]$$

Within the framework of the model, α and L can be obtained from Eq. [4]-[6], since

$$j_{w=0}/(dj/dw)_{w=0} = L \quad [7]$$

$$\ln(dj/dw) = \ln[KqI\alpha/(1 + \alpha L)] - \alpha w \quad [8]$$

with α obtained from the slope of the plot of $\ln(dj/dw)$ vs. w . Note that transformation of the experimentally accessible j vs. V to j vs. w plot requires knowledge of V_{FB} and N ; these can be obtained from a Mott-Schottky plot ($1/C^2$ vs. V) (7). In principle, the actual photocurrent-potential plots could be used in Eq. [7] and [8]. However, since the value of j at $w = 0$ can be very small, the values of L computed from directly measured j vs. V plots are inaccurate. Sukegawa *et al.* (6) developed the differential photocurrent (DPC) technique for obtaining the equivalent data for the determination of α and L .

Basis of DPC method.—The DPC method involves the modulation of the applied potential with a small amplitude (*e.g.*, 12 mVpp) sine wave at a frequency f_2 and the simultaneous modulation of the light intensity at a frequency f_1 with detection of the intermodulated photocurrent at $|f_2 - f_1|$. The intensity of the modulated light is maintained at a low level to prevent changes in dopant density and space-charge layer width from photoeffects alone (8). Figure 2 illustrates these principles. The small signal ac voltage brings about a change (Δw) in the space-charge layer width (w). This change in w produces a change in j , and this change in photocurrent, Δj , is represented by Eq. [5] (*i.e.*, $\Delta j/\Delta w$ approaches dj/dw for small depths of modulation). When the applied potential $V + V_0 \sin \omega_2 t$, where V_0 is the peak amplitude of the small superimposed ac voltage and $\omega_2 = 2\pi f_2$ is the ac angular frequency

$$\Delta w = \epsilon\epsilon_0 V_0 \sin(\omega_2 t) / qNw \quad [9]$$

In the course of one ac cycle, the maximum change in the scl width would be proportional to $2V_0$. However, a more meaningful value for use as the voltage change during a cycle would be the effective voltage or root-mean-square (rms) voltage. The peak-to-peak ac voltage ($2V_0$) is related to the rms voltage (V_{rms}) by

$$V_{\text{rms}} = 0.707 V_0 \quad [10]$$

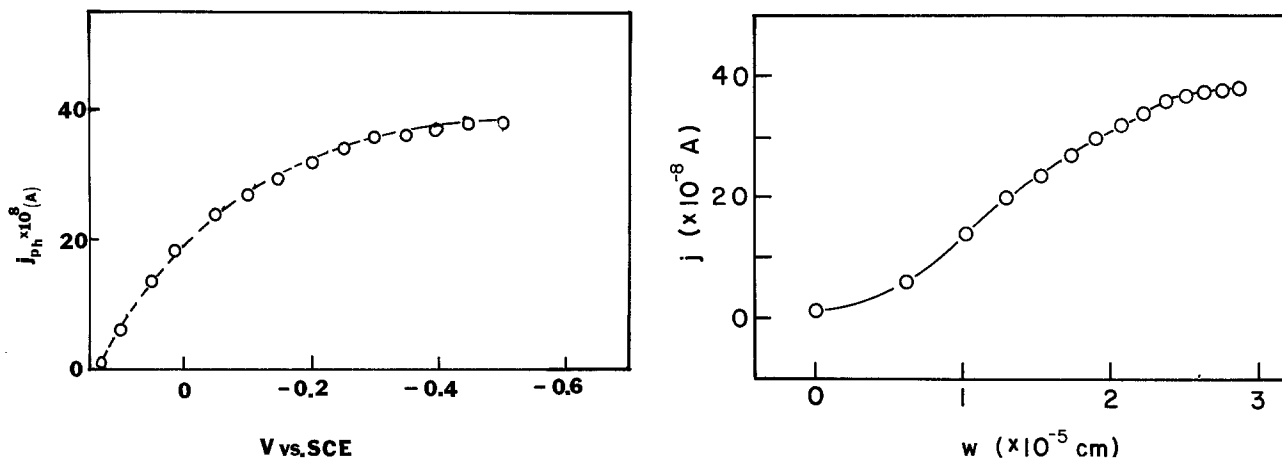


Fig. 1. A, left: plot of photocurrent (j) vs. applied dc bias (V) for a hypothetical case. B, right: plot of j vs. w , the space-charge layer width for the same case.

Hence, $2V_{\text{rms}}$ was employed in the computation of Δw from Eq. [3]. When the incident photon flux is modulated with angular frequency of $\omega_1 = 2\pi f_1$, the intensity of illumination varies as

$$I(t) = I_0(1 + m \sin \omega_1 t) \quad [11]$$

where m is the depth of modulation and $2I_0$ is the maximum incident photon flux. In our experiments, the depth of modulation can be set approximately equal to 100%, and, hence, Eq. [11] reduces to

$$I(t) = I_0(1 + \sin \omega_1 t) \quad [12]$$

It is evident from Eq. [1] that upon changing the space charge layer width w by Δw there is a corresponding change in j by Δj . This is expressed by the following relationship

$$\begin{aligned} J &= j + \Delta j = KqI \{1 - [e^{-\alpha(w+\Delta w)/(1+\alpha L)}]\} \\ &= KqI \{1 - [e^{-\alpha w/(1+\alpha L)}](e^{-\alpha \Delta w})\} \\ &= KqI \{1 - [e^{-\alpha w/(1+\alpha L)}](1 - \alpha \Delta w)\} \\ j + \Delta j &= KqI \{1 - [e^{-\alpha w/(1+\alpha L)}]\} \\ &\quad + KqI \alpha \Delta w e^{-\alpha w/(1+\alpha L)} \quad [13] \end{aligned}$$

Substitution of the time varying quantities $I(t)$ and

Δw from Eq. [12] and [9] into Eq. [13] gives the amplitude of the photocurrent, j , at ω_1

$$j(\omega_1) = KqI_0 [1 - e^{-\alpha w/(1+\alpha L)}] \quad [14]$$

and the differential photocurrent, Δj at Δw

$$\Delta j(\Delta w) = (KqI_0/2) [\alpha/(1+\alpha L)] (e^{-\alpha w}) (\epsilon_0 V_0 / qNw) \quad [15]$$

The derivations of Eq. [14] and [15] are given in the Appendix.

The values of Δw can be computed from Eq. [3] and [10] as a function of w .

Two lock-in amplifiers, one set at ω_1 and the other at $|\omega_1 - \omega_2|$, were used to detect the photocurrent; thus, both j (at ω_1) and Δj (at $|\omega_1 - \omega_2|$) can be recorded simultaneously. From the computed values of Δw and measured Δj , one can make a plot of $\ln(\Delta j/\Delta w)$ vs. w (Eq. [8]). The slope of the plot yields α at the wavelength of measurement. The Y-intercept of the plot, corresponding to $w = 0$, yields $[\Delta j/\Delta w]_{w=0}$. The value of α obtained previously, can be inserted in Eq. [1], and a plot of j vs. $e^{-\alpha w}$ extrapolated to $e^{-\alpha w} = 1$ (corresponding to $w = 0$) yields $[j]_{w=0}$. From these values, L can be computed from Eq. [7]. In addition to the DPC technique, a wealth of information pertaining to the experimental determination of L is available in the literature. These include the surface photovoltage technique (9-11), the electron bombardment of Schottky barriers (12), the photoluminescent-saturation measurement (13), and various other techniques (14-18). In most of these studies, one needs to know α to evaluate L . Since in many cases α is not known, it has to be determined separately, usually from absorbance measurements (19-24).

We report here DPC studies of single-crystal p-GaP and n-MoSe₂ semiconductors contacting liquid electrolytes containing $\text{Eu}^{3+/2+}$ and $\text{K}_4\text{Fe}(\text{CN})_6$, respectively, as redox couples. The adaptation of this method reported here has the advantage that the measurements are conducted with the semiconductor in the same configuration normally used in PEC cells, unlike the other techniques mentioned. One drawback, however, is that any deleterious effects the electrolyte has on the semiconductor, such as surface recombination or formation of surface states, could affect the measurement. An example of this is the absorption of light by redox couples. In solid-state measurements, no new chemical species are formed, and the light incident on the semiconductor is constant with respect to time. This is not necessarily the case with semiconductors in PEC cells. Species are generated at the photoelectrode with different absorption characteristics than the original form. If these generated species absorb at the wavelength of interest, errors will be caused by the time-

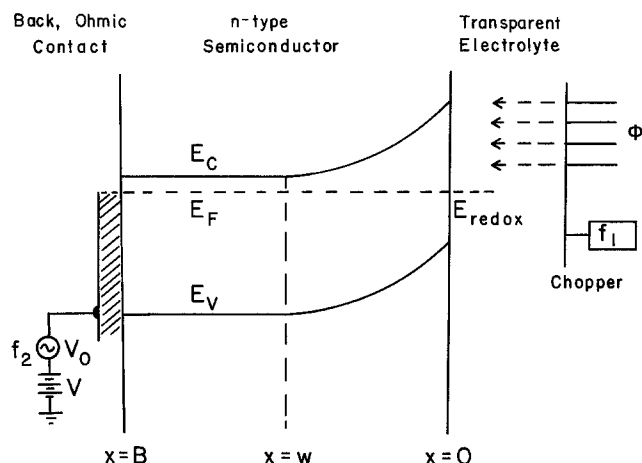


Fig. 2. Schematic of energy-band diagram illustrating the principle of measurement. Φ is the incident photon flux density chopped at an angular frequency of $\omega_1 = 2\pi f_1$; $2V_0$ is the peak-to-peak amplitude of the small signal ac voltage at an angular frequency of $\omega_2 = 2\pi f_2$; V is the applied dc reverse bias; $x = 0$, w , and B represent, respectively, the interface, space-charge layer width, and the back of the crystal where the ohmic contact is made; E_C = conduction bandedge; E_F = Fermi level; E_V = valence bandedge; E_{redox} = redox potential.

dependent filter effect. For this reason, as well as the good kinetics, $\text{Eu}^{3+/2+}$ and $\text{Fe}(\text{CN})_6^{3-/4-}$ were chosen as redox couples.

Experimental

The single-crystal semiconductors employed in this study were p-GaP and n-MoSe₂. The procedures for mounting and etching the electrodes are given elsewhere (25). The solution used with p-GaP was 0.1M EuCl_3 in 1M HClO_4 , and that used with n-MoSe₂ was 0.2M $\text{K}_4\text{Fe}(\text{CN})_6$ adjusted to pH 8 with KOH. Solutions were bubbled with prepurified N₂ prior to use, and N₂ was passed over the solutions during the experiment. A single-compartment electrochemical cell of 40 ml capacity with an optically flat window was used for all experiments. The counterelectrode was a large-area (40 cm²) Pt gauze, and the reference electrode was a saturated calomel electrode (SCE) with a KCl-saturated agar plug immersed directly into the cell. All potentials are expressed relative to the SCE unless otherwise specified.

A PAR Model 173 Potentiostat and a PAR Model 175 Universal Programmer (Princeton Applied Research Corporation, Princeton, New Jersey) were used to obtain the cyclic voltammograms, which were recorded on a Model 2000 X-Y recorder (Houston Instruments, Austin, Texas).

The ac impedance studies (26) utilized the lock-in amplifier technique, which yields the in-phase and the out-of-phase components of an ac signal superimposed on a dc voltage ramp. The ac signal (12 mV peak to peak) at different frequencies was obtained for input into the potentiostat from a Model 200 CD wide-range oscillator (Hewlett-Packard, Palo Alto, California). The output from the potentiostat, which was a voltage proportional to the current flowing between the working electrode (semiconductor) and the counterelectrode, was separated into its components at 0° and 90° with respect to the sine wave input by using a PAR Model 5204 lock-in amplifier and recorded with a Model 6432 (Soltec, Sun Valley, California) X-Y₁Y₂ recorder.

The experimental apparatus used for obtaining the differential photocurrent is shown in Fig. 3. A 2.5 kW Xe lamp (Schoeffel Instrument Company, Westwood, New Jersey) and monochromator (Jarrell-Ash Model 82560, Waltham, Massachusetts), with appropriate slits to achieve a bandpass of ~10 nm, were used as the

monochromatic light source. The light was modulated at 1111 Hz with a PAR Model 192 variable-frequency chopper. The ac frequency from the wide-band oscillator was adjusted to 1511 Hz with an amplitude of 12 mV peak to peak at the input of the potentiostat. A PAR Model 5204 lock-in amplifier was used to measure the photocurrent, j , which is the magnitude of the current present at the input of the lock-in with a frequency equal to the light chopping frequency, 1111 Hz. The much weaker (~1000×) differential photocurrent signal, Δj , was measured with a Model 5206 lock-in amplifier (EG&G, Princeton, New Jersey) equipped with an EG&G Model 5010 plug-in filter operated in the bandpass mode. The differential photocurrent is the magnitude of the current at the input of the lock-in with a frequency equal to the difference in the light chopping frequency and the ac modulation frequency, here arbitrarily kept at 400 Hz (1511 Hz - 1111 Hz). This signal was more conveniently recorded as $\log \Delta j$ by using the log of the magnitude output of the Model 5206. A reference signal for the lock-in at this beat frequency was obtained by passing f_1 from the chopper and f_2 from the oscillator, both adjusted to 0.8V peak to peak with voltage dividers, into the multiplier-filter circuit. The multiplier was constructed with an MC 1494L chip (Motorola, Incorporated) with the attendant circuitry as described in the product application information (27). The output, which consisted of a signal with frequency components at $f_1 + f_2$ and $f_2 - f_1$, was filtered to obtain only $f_2 - f_1$. This filter consisted of the bandpass output of a variable gain, state variable filter (28) constructed from an ECG 997 quad operational amplifier chip (Sylvania, Waltham, Massachusetts). Further filtering or amplification was found to be unnecessary for the reference channel of the EG&G 5206. Power for the circuit was supplied by a Harrison 6205B dual dc power supply (Hewlett-Packard). The potentiostat, programmer for dc ramp (2 mV/s), and X-Y₁Y₂ recorder were the same as mentioned previously.

As an independent check, L was determined by the surface photovoltage technique. The procedure used was that reported previously by Kamieniecki (29) and others (30). A tungsten-halogen lamp with power input controlled with an autotransformer was used as a light source. Monochromatic light was obtained with a grating monochromator (Model 7240, Oriel Corporation, Stamford, Connecticut). The lock-in amplifiers and

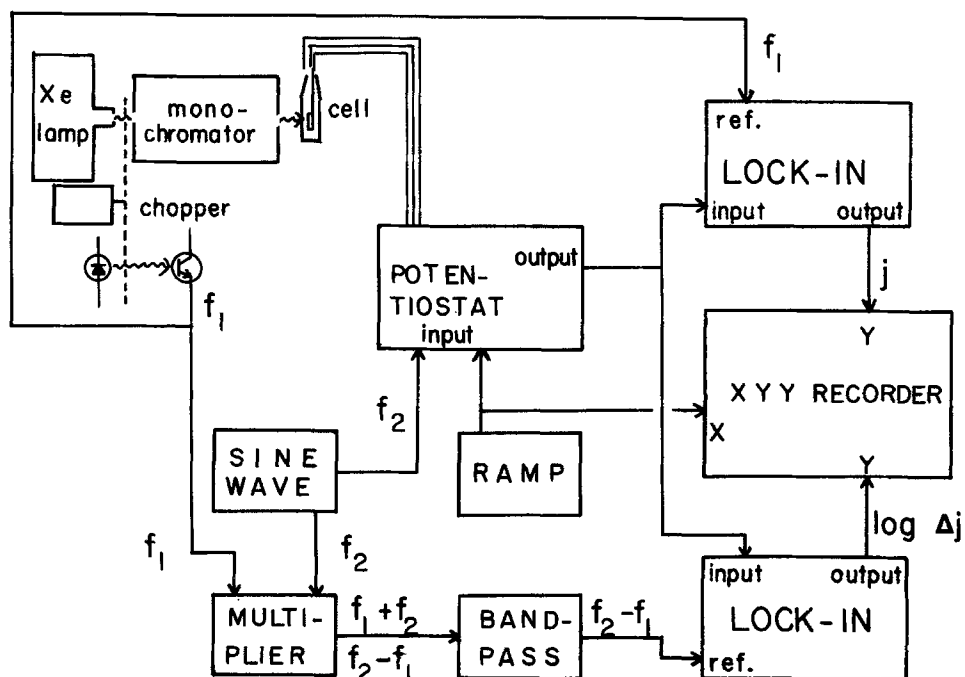


Fig. 3. Apparatus used for recording both the photocurrent (j) and the differential photocurrent (Δj). For details, see the Experimental section.

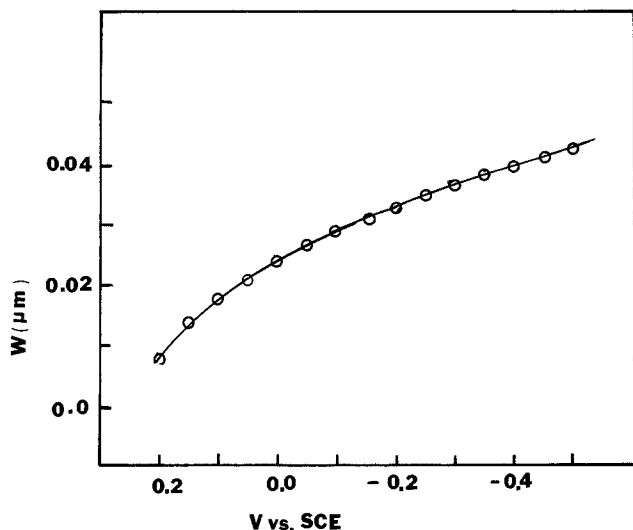


Fig. 4. Plot of the space-charge layer width as a function of applied bias for p-GaP in aqueous solutions containing Eu^{3+} as redox couple.

chopper are the same as previously described. The light intensity was monitored with a pyroelectric detector with a quartz window (Model P1-45Q, Molectron Corporation, Sunnyvale, California). In the surface photovoltage measurements, the solvent was acetonitrile (Spectrum Chemical Manufacturing Corporation, Gardena, California, spectrophotometric grade) and the electrolyte 0.01M tetra-n-butylammonium tetrafluoroborate (Southwestern Analytical Chemicals, Austin, Texas) which had been dried under vacuum at 100°C for 24h after recrystallization from acetone-ether. The solvent-electrolyte solution was stirred with activated alumina (Woelm Alumina N-Super I, Woelm Pharma GmbH and Company, Eschwege, Germany) decanted into the cell and deaerated and kept under a He atmosphere. The reference and counterelectrodes were the same as those used in the DPC measurement.

Results and Discussion

Computation of w and Δw .—For the determination of both w and Δw , one needs to know the value of N , the net doping density, and V_{FB} ; these can be obtained from the Mott-Schottky plot (7). The values of N and V_{FB} obtained from such a plot for p-GaP are $3.7 \times 10^{17} \text{ cm}^{-3}$ and $+0.22\text{V vs. SCE}$, respectively, in $\text{Eu}^{3+/2+}$ aqueous solution. The space-charge layer width, w , is related to N and V (where V is the applied potential) by Eq. [2]. Upon inserting the values of N and V into Eq. [2], the resulting plot of w vs. V for p-GaP in aqueous $\text{Eu}^{3+/2+}$ solution is obtained (Fig. 4). The values of Δw at different potentials were computed by Eq. [3]; the corresponding values of w were taken from Fig. 4. For computation of Δw , a value of $2V_{\text{rms}}$ instead of $2V_0$ was used. The reasons for this are discussed in detail above. The values of w and Δw from Eq. [2] and [3], respectively, are given in Table I as a function of V . Note, in Table I, that as the space-

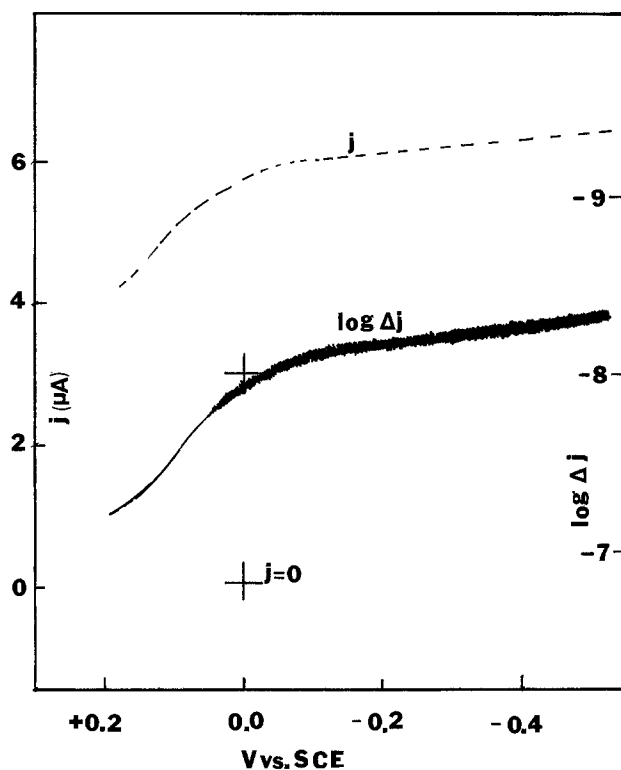


Fig. 5. j and Δj vs. V for p-GaP in aqueous solution containing Eu^{3+} as redox couple. The wavelength of irradiation is 400 nm. $f_1 = 1.111 \text{ kHz}$ and $f_2 = 1.511 \text{ kHz}$.

charge layer width increases, Δw decreases at a given ac modulation.

Plots of Δj and j vs. V .—Under reverse bias conditions, the dark current densities for the semiconductors used in this work were less than $1 \mu\text{A}$. Typical plots of Δj at $\Delta f = 400 \text{ Hz}$ (1511 – 1111 Hz) and j at 1111 Hz vs. applied bias, V , are given in Fig. 5 for p-GaP in aqueous solution containing $\text{Eu}^{3+/2+}$ as the redox couple. Frequencies 1111 and 1511 Hz correspond, respectively, to the chopping frequency f_1 , of the incident photon flux and the small signal ac frequency, f_2 , superimposed on the dc ramp, V . The plots in Fig. 5 are given for an incident photon energy of 3.1 eV (corresponding to 400 nm). The ordinate for the Δj (400 Hz) vs. V plot is given on a logarithmic scale. Similar results were obtained when the two modulating frequencies f_1 and f_2 were varied by $\pm 20\%$ while maintaining the Δf constant at 400 Hz for ease of filtering. Similar plots of Δj (400 Hz) and j were obtained for irradiation energies in the range 2.7–3.54 eV. Consider Fig. 5, where the photocurrent rises steadily reaching saturation around -0.1V . As j rises, Δj decreases monotonically tending to 0 at -0.1V where j reaches saturation.

Determination of α and L .—From the values of Δw in Table I and the Δj values at corresponding poten-

Table I. Typical values of w , Δw , Δj , and $\ln \Delta j/\Delta w$ for p-GaP in aqueous solution containing $\text{Eu}^{3+/2+}$ at two wavelengths

V (V vs. SCE)	$w \times 10^6$ (cm)	$\Delta w \times 10^{20}$ (m)	$\lambda = 400$ (nm)		$\lambda = 450$ (nm)	
			$\Delta j \times 10^9$ (A)	$\ln(\Delta j/\Delta w)$	$\Delta j \times 10^9$ (A)	$\ln(\Delta j/\Delta w)$
-0.5	4.253	2.504	4.786	2.950	1.000	1.384
-0.45	4.103	2.596	5.011	2.960	1.047	1.394
-0.4	3.947	2.699	5.248	2.967	1.097	1.402
-0.35	3.784	2.815	5.623	2.994	1.159	1.415
-0.3	3.614	2.947	5.888	2.994	1.245	1.440
-0.25	3.436	3.100	6.456	3.036	1.318	1.447
-0.2	3.248	3.279	6.606	3.002	1.413	1.460
-0.15	3.049	3.494	7.244	3.031	1.514	1.466
-0.1	2.835	3.757	7.943	3.051	1.660	1.485
-0.05	2.604	4.090	9.120	3.104	1.820	1.493

tials, from Fig. 5, plots of $\ln \Delta j/\Delta w$ vs. w were obtained (Fig. 6). The Δj and $\ln \Delta j/\Delta w$ values from these plots for p-GaP are given in Table I. A least squares fit was made for the computation of the slope and the Y-intercept. In this fit, a few points very close to V_{FB} were not included, since these points do not fall on the same line as data obtained at larger bias further into the depletion region. The reasons for the deviation are discussed below. The Y-intercept and the slope give, respectively, $(\Delta j/\Delta w)_{w=0}$ and the absorption coefficient, α . The α and $(\Delta j/\Delta w)_{w=0}$ at different wavelengths are given in Table II. This value of α is in good agreement with literature values (31), and is in the range 10^4 - 10^5 cm^{-1} at the wavelengths studied. The value of α at a particular wavelength was inserted into Eq. [1] and a plot of j vs. $e^{-\alpha w}$ obtained (Fig. 7). The j values corresponding to various selected potentials were obtained from Fig. 5. The $[j]_{w=0}$ obtained by extrapolating the plot in Fig. 7 to $e^{-\alpha w} = 1$ correspond-

ing to $w = 0$ at different wavelengths is given in Table II. The extrapolation was made by least squares analysis. Once again, for the least squares fit, values of j close to V_{FB} were neglected. The probable reasons for this positive deviation at small values of V can be attributed to a nonuniform doping density and near-surface recombination. If the impurity concentration is not uniform, w will be different in different regions of the semiconductor, since w varies as $N^{-1/2}$. For example, very close to the surface, if N is larger than the bulk doping density ($3.7 \times 10^{17} \text{ cm}^{-3}$), the actual value of w will be smaller than the computed one, giving a larger Δw . Moreover, if j rises sluggishly to saturation, the Δj will be larger than if j rises precipitously to saturation. The sluggish rise to saturation may be due to the recombination of photogenerated carriers. Thus, the larger Δj and smaller Δw can give rise to a positive deviation. No attempt was made, however, to account for this positive deviation, since one

Fig. 6. Plot of w (μm) vs. $\ln(\Delta j/\Delta w)$ for p-GaP in aqueous solution containing Eu^{3+} as redox couple; conditions are the same as in Fig. 5. Open circles represent data not used in the least squares fit.

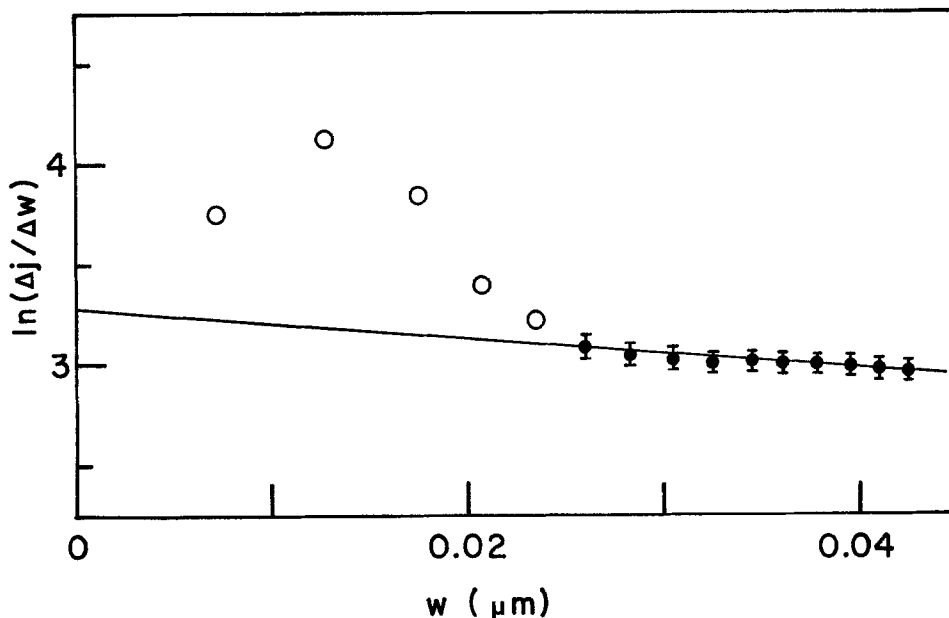


Fig. 7. Plot of $e^{-\alpha w}$ vs. j for p-GaP in aqueous solution containing Eu^{3+} as redox couple; conditions are the same as in Fig. 5.

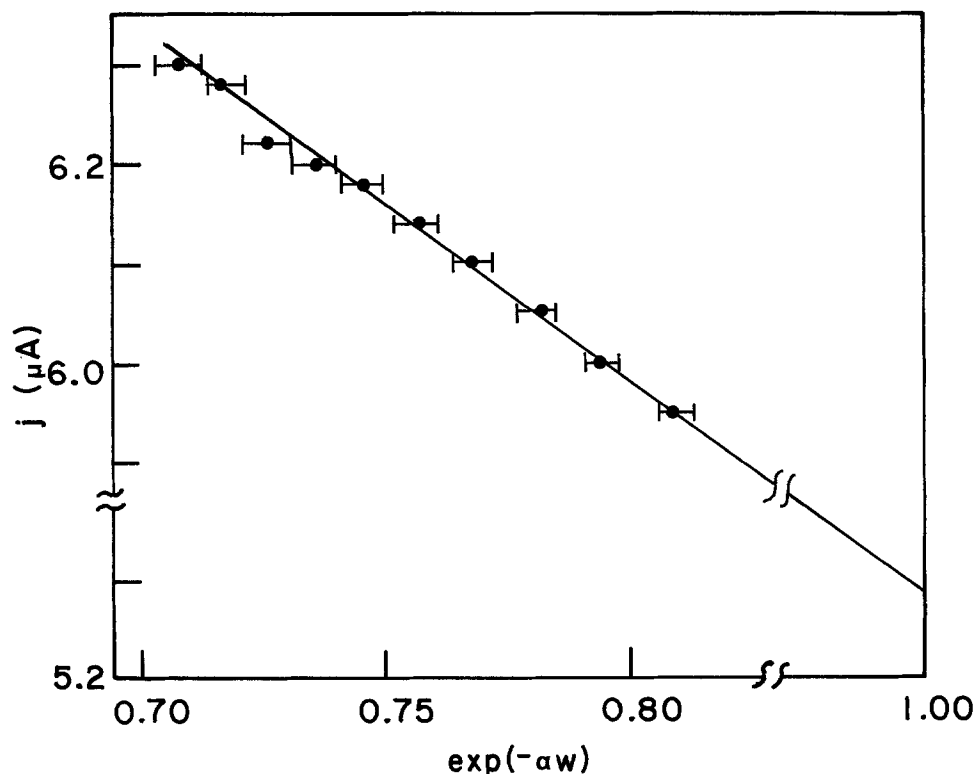


Table II. Values of α , L , and the parameters used to compute them; p-GaP; $\text{Eu}^{3+}/2+$

λ (nm)	α (cm^{-1})	$[\Delta j/\Delta\omega]_{\omega=0}$ (A/m)	$[j]_{\omega=0}$ (A)	L (μm)
450	6.9×10^4	5.35	1.09×10^{-6}	0.11
400	8.1×10^4	26.90	5.28×10^{-6}	0.10
350	3.6×10^5	142.33	10^{-7}	(~ 0.001)

needs to know the values of different parameters, such as surface recombination rate, bulk recombination rate, etc., under actual use conditions. Since these parameters are not easily determined, the values of j and $(\Delta j/\Delta\omega)$ close to V_{FB} were neglected.

The minority carrier diffusion length, L , was obtained from Eq. [7] from the values of $[j]_{\omega=0}$ and $(\Delta j/\Delta\omega)_{\omega=0}$. The values of L at different wavelengths are given in Table II. The literature values of L for p-GaP span a range 0.1–3 μm (15, 31). The minority carrier diffusion length, L , is related to the minority carrier lifetime, τ , and diffusion coefficient, D , by $L = (D\tau)^{1/2}$. The defects and the steps existing in the crystal can act as killer traps or recombination centers for minority carriers resulting in a drastic reduction in the minority carrier lifetime (32). Further, ions adventitiously incorporated into the lattice can also reduce the lifetime, τ . For example, Partin *et al.* (33) have shown that diffusion of cobalt into VPE n-GaAs_{0.6}P_{0.4} produced a considerable reduction of the diffusion length. Although L has been shown to be a function of doping density (15), the values of L obtained here ($\sim 0.1 \mu\text{m}$) are at the lower end of the range of values reported for similar doping densities. This suggests that the sample studied has a rather high number of recombination centers. Note that the value of L at 350 nm appears to be practically zero because the condition $\alpha\omega < 1$ is not satisfied. If $\alpha\omega > 1$, all the light will be absorbed within the space-charge layer with the result that there is no photocurrent attributable to diffusion of carriers from the semiconductor bulk.

Surface photovoltage measurement.—The value of L determined by the DPC technique was independently

checked by the surface photovoltage (SPV) technique (9–11, 29, 30). In this technique, the semiconductor electrode at open circuit is illuminated with chopped monochromatic radiation of energy slightly greater than the bandgap (E_g) of the semiconductor. The accumulation of minority carriers at the surface of the semiconductor produces a SPV. The SPV signal is capacitively coupled into the 10 Mohm impedance of a lock-in amplifier for amplification and measurement. The light intensity is adjusted to produce the same value of SPV at different wavelengths of excitation. The monochromatic light intensity required to produce this constant SPV signal is plotted against the reciprocal absorption coefficient for each wavelength. The α values for the wavelength range (500 nm – 440 nm) studied were those reported by Beckmann and Memming (34). The resultant linear plot is extrapolated to zero intensity, and the negative intercept value is the effective diffusion length. The results obtained by this technique are given in Fig. 8 for the same p-GaP sample studied by the DPC technique. The value of L obtained by least squares analysis of the data was $0.2 \pm 0.1 \mu\text{m}$. The uncertainty was the standard deviation of the values of L obtained from four different surface photovoltage values. The value of L agrees, within experimental uncertainty, with the value obtained by the DPC technique.

Effects of surface states on Δj - V behavior.—The claim by Sukegawa *et al.* (6) that this DPC technique is free from the effects of surface states does not appear to be valid. Surface states are known to affect the I-V behavior and may cause Fermi level pinning. These can be identified in different ways, including ac impedance measurements (26) and low frequency capacitance methods (35). We have studied the surface states on n-MoSe₂ in aqueous $\text{K}_4\text{Fe}(\text{CN})_6$ solutions by the ac conductance method (36). A typical plot of G_p (0° component) vs. V at 100 Hz is given in Fig. 9. The large hump in the range 0.1–0.45V can be attributed to the presence of surface states. DPC measurements were made with this electrode and plots of j and Δj vs. V are shown in Fig. 10. The dip in the Δj vs. V plot occurs in the same potential range in which G_p vs. V exhibits

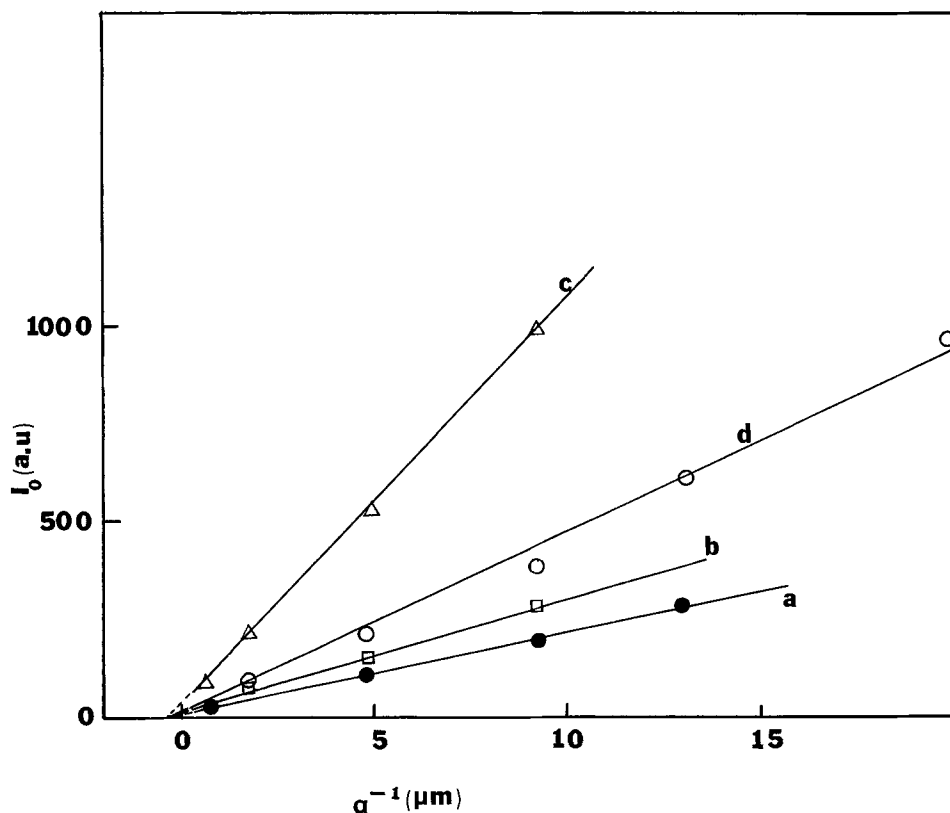
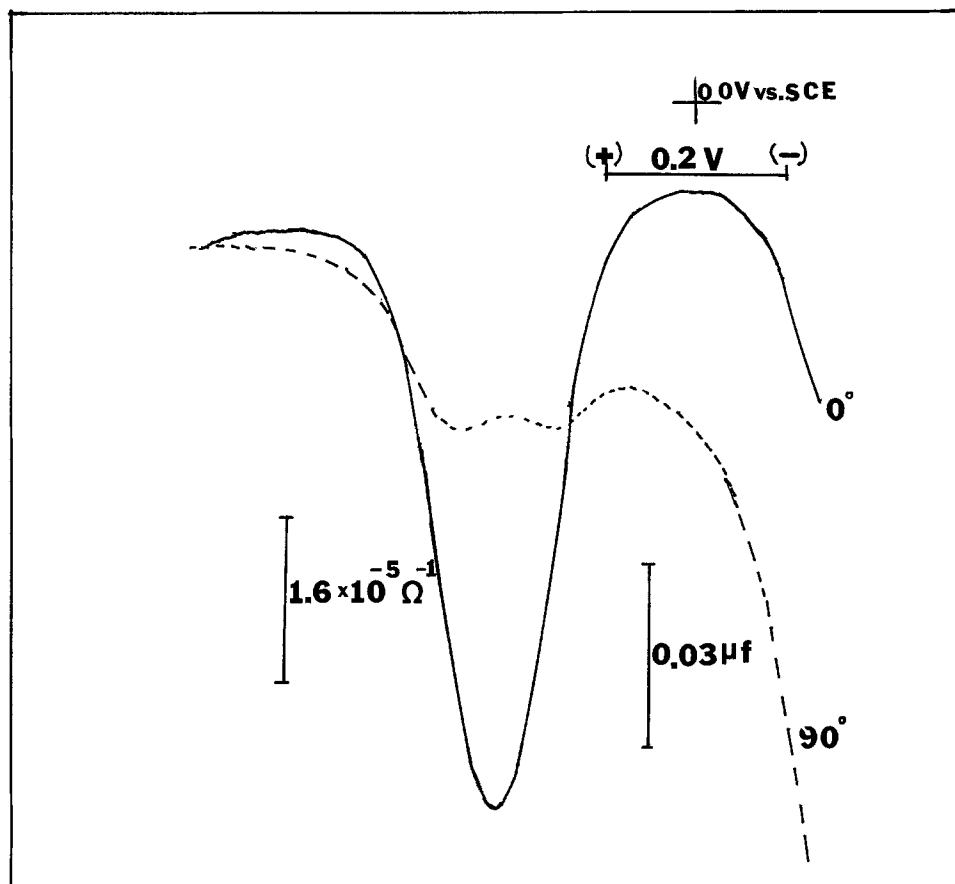


Fig. 8. Relative photon intensity (I_0 in arbitrary units) vs. inverse absorption coefficient (α^{-1}) for p-GaP in acetonitrile, 0.01M tetra-n-butylammonium tetrafluoroborate. Chopped at 87 Hz. Surface photovoltage was kept at: (a) 0.075 mV, (b) 0.1 mV, (c) 0.25 mV, and (d) 0.5 mV. The sensitivity of I_0 for SPV = 0.5 mV was $0.5 \times$ all others.

Fig. 9. G_p (in-phase component) vs. V for n-MoSe₂ in aqueous solution containing K₄Fe(CN)₆ as redox couple. $f = 100$ Hz.



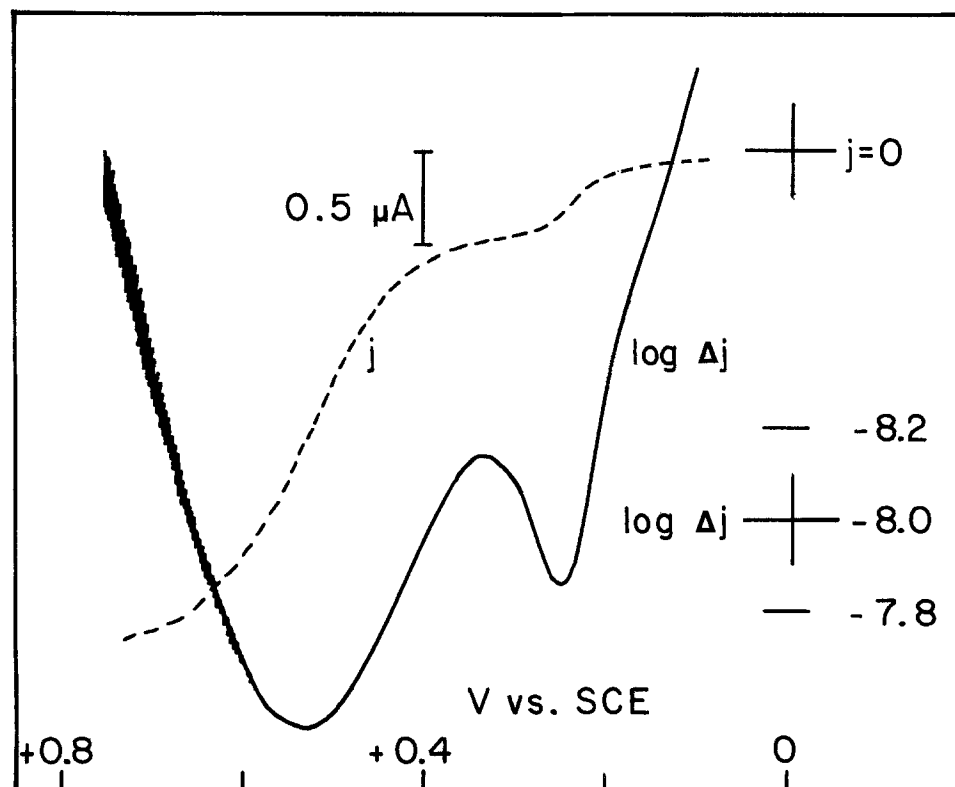
a hump; this dip is also ascribed to surface states. Consider the functional relationship between j and Δj . While j increases steadily, Δj decreases monotonically, and when $j \rightarrow j_{\text{sat}}$, $\Delta j \rightarrow 0$. However, when there is an inflection in the steady increase in j , there is a dip in the Δj vs. V plot. This inflection in the increase in j can be attributed to surface states acting as recombination centers. While the functional relationship between

j and Δj explains qualitatively the dip in Δj vs. V , a quantitative estimate of the density of surface states and the time constant of the surface states still needs to be addressed.

Conclusions

To our knowledge, this is the first time that the DPC method has been employed in liquid junction PEC cells. The absorption coefficient, α , for p-GaP is in the

Fig. 10. j and Δj vs. V for n-MoSe₂ in aqueous solution containing K₄Fe(CN)₆ as redox couple. The wavelength of irradiation is 500 nm. Modulation frequencies: $f_1 = 1.111$ kHz and $f_2 = 1.511$ kHz.



range 10^4 - 10^5 cm^{-1} in the wavelength range studied. This is in good agreement with that reported in the literature. However, L for our p-GaP is much smaller than the literature value for good-quality GaP crystals. This may be due to the existence of steps, defects, or incorporated metal ions. Finally, the results on n-MoSe₂ suggests that this method can be used to locate and identify surface states. The DPC method cannot be used in liquid junction PEC cells to determine α and L when surface states are present, the semiconductor decomposes under optical illumination, or the diffusion length is larger than the width of the crystal. These three factors precluded the measurement of α and L for Si, GaAs, and InP by this method in PEC cells.

Acknowledgments

The support of this work by the Solar Energy Research Institute and the National Science Foundation (CHE8304666) is gratefully acknowledged. B. L. W. wishes to acknowledge the generous support of The Electrochemical Society in the form of the Colin Garfield Fink Summer Fellowship.

Manuscript submitted July 22, 1983; revised manuscript received Dec. 28, 1983.

The University of Texas assisted in meeting the publication costs of this article.

APPENDIX

Introduction of the expression for the two modulated quantities, illumination ($I(t)$, Eq. [12]) and Δw (expressed as applied voltage, Eq. [9b]) into Eq. [13] leads to the total time dependent photocurrent.

$$J(t) = KqI_0(1 + \sin \omega_1 t) [1 - e^{-\alpha w} / (1 + \alpha L)] \\ + KqI_0(1 + \sin \omega_1 t) [e^{-\alpha w} \alpha / (1 + \alpha L)] \\ [(\epsilon_0 / qNw) V_0 \sin \omega_2 t] \quad [\text{A-1}]$$

or collecting terms

$$J(t) = KqI_0(1 + \sin \omega_1 t) [1 - e^{-\alpha w} / (1 + \alpha L)] \\ + KqI_0 [\alpha / (1 + \alpha L)] (e^{-\alpha w} \epsilon_0 V_0 / qNw) \\ \times [\sin \omega_2 t + (\sin \omega_1 t) \sin \omega_2 t] \quad [\text{A-2}]$$

From trigonometric identity

$$\sin A (\sin B) = 1/2[\cos(A - B) - \cos(A + B)]$$

Equation [A-2] can be rewritten as

$$J(t) = KqI_0(1 + \sin \omega_1 t) [1 - e^{-\alpha w} / (1 + \alpha L)] \\ + KqI_0 [\alpha / (1 + \alpha L)] (e^{-\alpha w} \epsilon_0 V_0 / qNw) \times [\sin \omega_2 t \\ + 1/2[\cos(\omega_1 - \omega_2)t - \cos(\omega_1 + \omega_2)t]] \quad [\text{A-3}]$$

Of the various signals present in the second term in Eq. [A-3], the major difference frequency component ($|\omega_2 - \omega_1|$) can be separated using a lock-in amplifier. The first term on the right-hand side in Eq. [A-3] is proportional to the photocurrent j , and the amplitude is given by

$$j(\omega_1) = KqI_0 [1 - e^{-\alpha w} / (1 + \alpha L)] \quad [\text{A-4}]$$

The amplitude of the major difference frequency ($|\omega_2 - \omega_1| = \Delta\omega$) component, the second term on the right-hand side in Eq [A-3] is expressed as

$$\Delta j(\Delta\omega) = (KqI_0/2) [\alpha / (1 + \alpha L)] e^{-\alpha w} \epsilon_0 V_0 / qNw \quad [\text{A-5}]$$

Dividing Eq. [A-4] by Eq. [A-5] gives

$$j_{w=0} / [\Delta j / \Delta w]_{w=0} = KqI_0 L [\alpha / (1 + \alpha L)] \\ / [(1/2) KqI_0 \alpha / (1 + \alpha L)] = 2L$$

Therefore

$$L = j_{w=0} / 2[\Delta j / \Delta w]_{w=0}$$

REFERENCES

- W. W. Gärtner, *Phys Rev.*, **116**, 84 (1959).
- M. A. Butler, *J. Appl. Phys.*, **48**, 1914 (1977).
- J. Reichman, *Appl. Phys. Lett.*, **36**, 574 (1980).
- H. Reiss, *This Journal*, **125**, 937 (1978).
- (a) R. H. Wilson, *J. Appl. Phys.*, **48**, 4292 (1977); (b) D. Laser and A. J. Bard, *This Journal*, **123**, 1833 (1976).
- T. Sukegawa, T. Watanabe, T. Mizuki, and A. Tanaka, *IEEE Trans. Electron Devices*, ed-27, 1251 (1980).
- G. Nagasubramanian, B. L. Wheeler, F-R. F. Fan, and A. J. Bard, *This Journal*, **129**, 1742 (1982).
- J. A. Turner and A. J. Nozik, *Appl. Phys. Lett.*, **41**, 101 (1982).
- E. Y. Wang, C. R. Baraona, and H. W. Brandhorst, Jr., *This Journal*, **121**, 973 (1974).
- S. S. Li, *Appl. Phys. Lett.*, **29**, 126 (1976).
- W. E. Phillips, *Solid-State Electron.*, **15**, 1097 (1972).
- C. J. Wu and D. B. Wittry, *J. Appl. Phys.*, **49**, 2827 (1978).
- C. J. Hwang, *J. Appl. Phys.*, **40**, 3731 (1969).
- B. L. Smith and M. Abbott, *Solid-State Electron.*, **15**, 361 (1972).
- P. D. Dapkus, W. H. Hackett, Jr., O. G. Lorimer, G. W. Kammlott, and S. E. Haszko, *Appl. Phys. Lett.*, **22**, 227 (1973).
- M. L. Young and D. R. Wight, *J. Phys. D*, **7**, 1824 (1974).
- E. H. Stupp and A. Milch, *J. Appl. Phys.*, **48**, 282 (1977).
- R. J. Lender, S. Tiwari, J. M. Borrego, and S. K. Ghandhi, *Solid-State Electron.*, **22**, 213 (1979).
- F. Bassani, in "Optical Properties of Solids," E. D. Haidemenakis, Editor, pp. 4-6, Gordon and Breach, Science Publishers, New York (1970).
- F. Bassani and G. Pastori Parravicini, "Electronic States and Optical Transitions in Solids," p. 153, Pergamon Press, New York (1975).
- A. V. Nurmikko, D. J. Epstein, and A. Linz, in "Optical Properties of Highly Transparent Solids," S. S. Mitra and B. Bendow, Editors, pp. 443-449, Plenum Press, New York (1975).
- J. Tauc, in "Proceedings of the International School of Physics 'Enrico Fermi.' Course 34. The Optical Properties of Solids," J. Tauc, Editor, pp. 63-89, Academic Press, New York (1966).
- A. J. Bard and L. R. Faulkner, "Electrochemical Methods. Fundamentals and Applications," p. 586, John Wiley and Sons, New York (1980).
- W. C. Dash and R. Newman, *Phys. Rev.*, **99**, 1151 (1955).
- (a) P. A. Kohl, S. N. Frank, and A. J. Bard, *This Journal*, **124**, 225 (1977); (b) F-R. F. Fan and A. J. Bard, *ibid.*, **128**, 945 (1981).
- G. Nagasubramanian, B. L. Wheeler, G. A. Hope, and A. J. Bard, *ibid.*, **130**, 385 (1983).
- "Motorola Linear Integrated Circuits, Series C," pp. 6-60-6-73, Motorola Inc. (1979).
- D. Lancaster, "Active Filter Cookbook," pp. 156-162, Howard W. Sams and Co., Inc., Indianapolis, IN (1975).
- E. Kamieniecki, *J. Vac. Sci. Technol.*, **20**, 811 (1982).
- "Annual Book of ASTM Standards," pp. F391-73T, ASTM, Philadelphia, PA (1975).
- (a) M. L. Young and D. R. Wight, *J. Phys. D*, **7**, 1824 (1974); (b) B. L. Smith and M. Abbott, *Solid-State Electron.*, **15**, 361 (1972); (c) S. A. Abagyan and V. K. Subashiev, *Sov. Phys. Solid State*, **6**, 2529 (1965); (d) V. K. Subashiev and G. A. Chalikian, *Phys. Status Solidi*, **13**, K91 (1966).
- H. J. Lwernerz, A. Heller, and F. J. Disalvo, *J. Am. Chem. Soc.*, **102**, 1877 (1980).
- D. L. Partin, A. G. Milnes, and L. F. Vassamillet, *This Journal*, **126**, 1584 (1979).
- K. H. Beckmann and R. Memming, *ibid.*, **116**, 368 (1969).
- K. Kobayashi, Y. Aikawa, and M. Sukigara, *Chem. Lett.*, 679 (1981).
- G. Nagasubramanian, B. L. Wheeler, and A. J. Bard, *This Journal*, **130**, 1680 (1983).